

# AKARI observation of the fluctuation of the near-infrared background. I.

T. Matsumoto<sup>1,2</sup>, H. J. Seo<sup>1</sup>, W. -S. Jeong<sup>3</sup>, H. M. Lee<sup>1</sup>, S. Matsuura<sup>2</sup>, H. Matsuhara<sup>2</sup>, S. Oyabu<sup>2,4</sup>, and T. Wada<sup>2</sup>

matsumo@ir.isas.jaxa.jp

Received \_\_\_\_\_; accepted \_\_\_\_\_

---

<sup>1</sup>Department of Physics and Astronomy, Seoul National University, Seoul 151-742, Korea

<sup>2</sup>Department of Infrared Astrophysics, Institute of Space and Astronautical Science (ISAS), Japan Aerospace Exploration Agency (JAXA), Sagamihara, Kanagawa 252-5210, Japan

<sup>3</sup>Korea Astronomy and Space Science Institute (KASI), Daejeon 305-348, Korea

<sup>4</sup>present address: Department of Physics, Nagoya University, Nagoya 464-8601, Japan

## ABSTRACT

We sought to detect fluctuations of brightness in the sky toward the north ecliptic pole (NEP) with the Japanese infrared astronomical satellite AKARI, at 2.4, 3.2, and 4.1  $\mu\text{m}$ . The obtained circular maps with 10 arcmin diameter clearly show a spatial structure on the scale of a few hundred arcseconds, which is consistent with observations by NASA’s Spitzer Space Telescope. The power spectrum analysis shows that there is a significant residual fluctuation at angular scales larger than 100 arcseconds that can’t be explained by zodiacal light, diffuse galactic light, shot noise of faint galaxies or clustering of low redshift galaxies. These findings indicate that the detected fluctuation could be attributed to the pop. III stars, that is, first stars of the universe. Observed fluctuating component at large angular scales has a blue stellar spectrum. We determine correlations between wavelength bands whose color is roughly similar to the spectrum of the fluctuating component. The obtained spatial structure and power spectrum are consistent with the theoretical prediction, biased star formation of the pop.III stars which follows density distribution of the dark matter.

*Subject headings:* cosmology: observations — fluctuation — first stars — infrared: diffuse background

## 1. Introduction

A search for the cosmic near-infrared background has been commenced using data from the Cosmic Background Explorer (COBE) (Hauser et al. 1998; Cambr  sy et al. 2001; Arendt & Dwek 2003; Levenson et al. 2007) and the Infrared Telescope in Space (IRTS) (Matsumoto et al. 2005). The results have consistently shown that there remains an isotropic emission that can hardly be explained by known sources. One possible origin of this excess emission is population (pop.) III stars that caused reionization of the universe (Salvaterra & Ferrara 2003; Dwek et al. 2005). The obtained excess emission, however, is much brighter than expected, and requires vast amount of star formation during the pop. III era (Madau & Silk 2005). Furthermore, TeV- $\gamma$  observations of distant blazars favor a low-level near-infrared extragalactic background light (Aharonian et al. 2006). It has been pointed out that the uncertainty in the model of zodiacal light may lead to ambiguity in the result. In order to obtain firm results on the near-infrared cosmic background, fluctuation measurement has attracted researcher’s attraction, since zodiacal light is very smooth. Recently, Kashlinsky et al. (2005, 2007) reported significant fluctuations at angular scales of 100~300 arcseconds based on Spitzer data and concluded that they were caused by pop. III stars. However, a few researchers have claimed that the origin of this fluctuation was the clustering of low redshift galaxies (Cooray et al. 2007; Sullivan et al. 2007; Chary et al. 2008). Thompson et al. (2007b) detected a significant fluctuation at 1.1  $\mu\text{m}$  and 1.6  $\mu\text{m}$  based on the Near-Infrared Camera and Multi-object Spectrometer (NICMOS)/Hubble Space Telescope (HST) data, although their observation was restricted to angular scales of smaller than 100 arcseconds. In this paper, we present new observations on fluctuations in sky brightness using Japanese infrared astronomical satellite AKARI, which has a cold shutter to measure dark images precisely as well as a short wavelength band at 2.4 $\mu\text{m}$ , which provided new observational evidences on the study of the sky fluctuation.

## 2. Observations and data reduction

AKARI is the Japanese infrared astronomy satellite launched on February 22, 2006 (Murakami, et al. 2007). AKARI monitored a fixed position in the sky near the north ecliptic pole (NEP) ( $\alpha_{2000}=17^{\text{h}}55^{\text{m}}24^{\text{s}}$ ,  $\delta_{2000}=66^{\circ}37'32''$ ) to confirm the performance of the Infrared Camera (IRC) (Onaka et al. 2007). Pointing observations were carried out twice a month and 2-3 images were taken for all filter bands during one pointing observation. To detect the fluctuations in sky brightness, we used near-infrared images taken between September 2006 and March 2007 during which no radiation from the earth entered the baffle and stray light was negligible. The near-infrared camera has a frame of 10 arcminute square with a pixel scale of 1.5 arcseconds. After applying ordinary pipeline procedures (Lorente et al. 2008), we selected 40, 39, and 28 high quality images for 2.4, 3.2, and 4.1  $\mu\text{m}$  bands, respectively (hereafter we list data at these three bands in order of wavelength). The total integration times were 29.6, 28.9, and 20.7 minutes. We stacked these images and obtained the final fluctuation maps on the NEP field. Due to the constraint of attitude control, the position angle of the image rotated by 200 degrees during the observation period, resulting in circular images with 10 arcminute diameters. This improves the quality of the sky maps compared to usual stacking, since flat field errors, fluctuations in sensitivity between pixels, fluctuations of the zodiacal light (if any), etc., are smoothed out. We also obtained 25 dark frames with the cold shutter closed and obtained stacked dark maps for the three bands by applying the same procedure used for image frames.

In order to obtain the fluctuations in sky brightness, we masked the pixels whose signal exceeded a level of  $2\sigma$ . We repeated this 10 times as this was sufficient to prevent further iteration from producing any changes to the final result. However, there remained bright pixels around masked region because of the extended point spread function (PSF). To subtract this effect, we detected foreground sources for the unmasked stacked images using

the DAOFIND task in the Image Reduction and Analysis Facility (IRAF) to as faint an end as possible, and sought to remove their contributions. As for the point sources, we estimated the contribution of sources at outer region using a carefully modeled PSF and subtracted them from sky images. We obtained PSF based on the beam profiles of the bright point sources, which were optimized so that the edge of the masked region had the same sky brightness as the neighboring sky. We identified extended objects using ground-based data for the NEP region (Imai et al. 2007) which has a better spatial resolution. We created convolved images with the AKARI’s PSF and subtracted them from sky images. For these PSF subtracted images, we masked the same region as that of  $2\sigma$  clipping image. In order to minimize contributions from PSFs, we further masked a layer of one pixel around the masked region. Even after these procedures, there remained identified sources that were not masked in  $2\sigma$  clipping process. We simply masked the 8 neighboring pixels around their centers. For the dark maps, we first normalized them so that they had the same statistical weights as the sky images, assuming a Gaussian distribution. We masked the same region as sky maps and repeated  $2\sigma$  clipping 10 times.

Upper and middle panels in Fig.1 indicate sky maps and dark maps, respectively. Sky maps clearly show structure, while dark maps look like random noise. Percentages of remaining pixels are 39.8, 39.3, and 36.8 %. Average sky brightness are 122, 75, and 103  $\text{nWm}^{-2}\text{sr}^{-1}$ . Standard deviations for sky maps are 2.25, 1.34, and 0.72  $\text{nWm}^{-2}\text{sr}^{-1}$ , while those for dark maps are 1.49, 0.89, and 0.42  $\text{nWm}^{-2}\text{sr}^{-1}$ .

Although systematic errors due to the absolute calibration were 2.8, 2.5, and 3.4 % (Lorente et al. 2008), throughout this paper, we present all data without systematic errors in order to reveal fluctuations clearly.

### 3. Power spectrum

To examine the nature of the fluctuations, we obtained power spectra  $[q^2 P_2 / (2\pi)]^{1/2}$  as a function of wave number  $q$  using two-dimensional Fourier transformation for both the sky and dark maps, following the analysis of previous authors (Thompson et al. 2007a). Upper panel of Fig.2 shows a power spectrum on the angular scale  $(2\pi)/q$  for both the sky (filled circles) and dark (open triangles) maps. Power spectra of sky maps show significantly larger power than those of dark maps.

We performed a subset analysis to confirm the celestial origin of the observed structure. We divided the original images alternately in a time sequence into two subsets and obtained two stacked images, F1 and F2, by applying the same procedure as that described in the previous section. The power spectra of the difference between these two images are shown as open squares in upper panel of Fig.2. The results are fairly consistent with those of the stacked dark images. This indicates that the observed structure commonly exists in the original images and is of a celestial origin.

We subtracted the power spectrum of the dark maps from that of the sky maps in quadrature, the result of which are shown as filled circles in lower panel of Fig.2. The solid lines show the power spectra due to shot noise of faint galaxies that were obtained by simulation. The decline at small angle is caused by the PSF, while absolute value depends on the limiting magnitude and galaxy counts. We used galaxy counts that were obtained for the stacked images before masking and extended to the faint end assuming a slope of 0.23 for logarithmic counts (Maihara et al. 2001). The power spectra of the shot noise of faint galaxies were well fitted to the observed power spectra with the limiting magnitudes (AB), 22.9, 23.3, and 24.0. Fig.2 shows that a significant residual power remains over the shot noise at large angular scales.

Lower panel of Fig.1 shows smoothed sky maps that were obtained by taking averages

within a 50 arcseconds diameter circle centered at each pixel. The smoothed maps clearly show the existence of a significant extended spatial structure with an angular scale of a few hundred arcseconds for all wavelength bands. This is consistent with excess power at large angular scales shown in Fig. 2. This structure is significant since they are absent from the smoothed dark maps. The  $1\sigma$  fluctuations of the smoothed sky maps after subtracting those of the smoothed dark maps in quadrature were 0.53, 0.23, and 0.19  $\text{nWm}^{-2}\text{sr}^{-1}$ .

In order to examine the fluctuation qualitatively, we took the average of the fluctuating power for 7 points at angular scales between 100 and 350 arcseconds (filled circles in Fig.3). The characteristic feature of Fig.3 is that the fluctuating component has a very blue-star-like spectrum. Color for 2.4 and 3.2  $\mu\text{m}$  is consistent with Rayleigh-Jeans spectrum (straight line in Fig.3). Open squares show the Spitzer results (Kashlinsky et al. 2005, 2007), which agree with ours. At wavelength bands of 1.1 and 1.6  $\mu\text{m}$ , Thompson et al. (2007b) detected fluctuating powers of 0.3 and 0.4  $\text{nWm}^{-2}\text{sr}^{-1}$ , respectively, at an angular scale of 85 arcseconds. These are lower than the values extrapolated from the AKARI data, assuming the Rayleigh-Jeans spectrum. However, the angular scale for NICMOS/HST is too small to have detected the large-scale structure shown in the smoothed maps. Therefore, we consider it inappropriate to compare NICMOS/HST results directly with ours. Finally, we note that the excess isotropic emission observed by IRTS (Matsumoto et al. 2005) has a spectrum similar to the present study.

Fig.4 shows correlation diagrams for three bands. The correlation between 3.2 and 2.4  $\mu\text{m}$  is fairly strong (correlation coefficient  $\sim 0.8$ ), while that between 4.1 and 2.4  $\mu\text{m}$  is somewhat weak (correlation coefficient  $\sim 0.5$ ). Spectrum of the correlating component normalized to those at 2.4  $\mu\text{m}$  is also plotted as open circles in Fig.3. Although the overall spectrum of the correlating component is similar to that of large scale fluctuation (filled circles), the error for the 4.1  $\mu\text{m}$  band is relatively large. This is consistent with the result

that the smoothed map for  $4.1\ \mu\text{m}$  shows a somewhat different structure from those for  $3.2\ \mu\text{m}$  and  $2.4\ \mu\text{m}$ .

#### 4. Origin of fluctuation

As the main component of sky brightness, zodiacal light is a candidate for the origin of the fluctuation. The subset analysis constitutes clear evidence that zodiacal light is not the source of the observed fluctuation. Since its position varied due to the revolution of the earth, AKARI detected both temporal and spatial fluctuations of zodiacal light. If the observed fluctuation were caused by zodiacal light, the difference between the two subsets should have shown much larger fluctuating power than that for dark images.

Fluctuation levels detected are also higher than those expected for zodiacal light. IRAS (Vrtilek & Hauser 1995), COBE (Kelsall et al. 1998) and ISO (Abraham et al. 1999) attempted to detect the fluctuation of zodiacal emission and obtained upper limits of 1 % for the angular scales from arcminutes to degrees. Recently, Pyo et al. (2010) analyzed the zodiacal light and emission using the same data set as that we used in this paper, and obtained upper limits of their fluctuations for the angular scale larger than 100 arcsec. In near-infrared bands, upper limit is  $\sim 0.3\%$ , while that in mid-infrared bands is  $\sim 0.04\%$ . Since it is reasonable to assume that fluctuation of zodiacal light is similar to that of zodiacal emission, we applied the upper limit of the fluctuation of zodiacal light to be 0.04 %. Expected fluctuation of zodiacal light is significantly reduced during the stacking procedure by a factor equal to the inverse square root of the number of stacked images, which provides upper limits to be 0.0063%, 0.0064 %, and 0.0076% for the 2.4, 3.2, and  $4.1\ \mu\text{m}$  band, respectively. The sky brightness corresponding to these upper limits is 0.0077, 0.0048, and  $0.0078\ \text{nWm}^{-2}\text{sr}^{-1}$ . They are significantly lower than the observed fluctuation powers at large angular scales, 0.19, 0.080, and  $0.051\ \text{nWm}^{-2}\text{sr}^{-1}$  in Fig.3. Therefore, we



conclude that the contribution of zodiacal light to the fluctuation is negligible.

The second possible origin of the fluctuation is diffuse galactic light (DGL), scattered starlight and thermal emission of interstellar dust. Since DGL is closely related to the dust column density, we examined its correlation with far-infrared emission ( $90\ \mu\text{m}$ ) observed with the Far-Infrared Surveyor (FIS)/AKARI (Matsuura et al. 2010) for  $\sim 30$  arcseconds angular resolution. Fig.5 shows no significant correlation between near-infrared and far-infrared fluctuation, indicating that DGL is not the source of the observed near-infrared fluctuation.

The third candidate is the clustering of faint galaxies. A few authors (Cooray et al. 2007; Sullivan et al. 2007; Chary et al. 2008) have claimed that the fluctuation observed by Spitzer is due to the clustering of low redshift galaxies. The blue color observed here directly rejects the proposal by Chary et al. (2008) that the fluctuating component originates in red dwarf galaxies. Sullivan et al. (2007) examined the contribution of the clustering of faint galaxies to the sky fluctuation. Based on their work, we estimated the power due to the clustering of galaxies fainter than the limiting magnitude of this study at multipole,  $l \sim 1,000$  ( $\sim 600$  arcseconds), to be  $\sim 0.03\ \text{nWm}^{-2}\text{sr}^{-1}$ . This is significantly lower than the power observed by AKARI at  $2.4\ \mu\text{m}$ . At the L band, Fig.8 in Sullivan et al. (2007) shows that fluctuating power due to clustering is fairly low compared with that observed by Spitzer (Kashlinsky et al. 2005, 2007). These evidences indicate that the clustering of low redshift faint galaxies is not likely to be the source of the observed fluctuation.

Totani et al. (2001) estimated contribution of the faint galaxies to the background, and found integrated brightness of galaxies at the K band amounts to  $7.8 \pm 1.2\ \text{nWm}^{-2}\text{sr}^{-1}$ . Galaxies of  $\sim 18$  mag are most responsible for the integrated brightness, and the fainter galaxies than that render less contribution. Integrated brightness at  $2.4\ \mu\text{m}$  due to galaxies

fainter than limiting magnitude of 22.9 mag is estimated to be at most  $1 \text{ nWm}^{-2}\text{sr}^{-1}$ , assuming a slope of 0.23 for logarithmic counts (Maihara et al. 2001). Observed fluctuating power at large angular scales is a fraction of this brightness, which is fairly large. This situation is more conspicuous for the case of NICMOS/HST observation (Thompson et al. 2007b), since their limiting magnitudes are much lower than the AKARI observation. In case of the H band, estimated integrated brightness due to galaxies fainter than 28.5 mag is  $0.1 \text{ nWm}^{-2}\text{sr}^{-1}$ , which is significantly lower than observed fluctuation,  $0.4 \text{ nWm}^{-2}\text{sr}^{-1}$ . These considerations imply that a simple extrapolation of galaxy counts hardly explains observed fluctuating power, and suggest there must exist a new population of infrared sources at the faint end.

To summarize, we found that the observed near-infrared fluctuation at large angular scale can hardly be explained by known sources. We regard that the most probable origin of the fluctuation, therefore, is pop. III stars.

## 5. Discussions

AKARI observations have shown that there existed a large scale structure even at pop.III era. Since power spectrum is still flat at 10 arcmin scale, large scale structure at pop.III era could be more extended. The co-moving distance for 10 arcmin at  $z \sim 10$  is  $\sim 30$  Mpc. It must be noted that this is similar to large scale structure in the present universe.

Cooray et al. (2004) presented the first theoretical study on the fluctuations caused by pop. III stars. They assumed biased star formation which traces the density distribution of dark matter. Although absolute level of fluctuating power has a wide range depending on the parameters, overall shapes have almost same convex feature with a flat peak at  $l \sim 1,000$  ( $\sim 10$  arcmin) and a turn over toward large angle. We attribute the excess power

observed with AKARI to this flat peak. The fluctuating power observed with AKARI is marginally consistent with pessimistic estimate. The spectrum of fluctuating power of the model is fairly blue which basically agrees with AKARI observation. Observed fluctuation with AKARI could be interpreted within the framework of this model. However, detection of turn over at larger angles than 10 arcmin is essential.

Recently, Fernandez et al. (2010) made a numerical simulation of the cosmic near-infrared background due to early populations (pop. II and III stars) assuming halo mass of  $2 \times 10^9$  solar mass. They calculated both amplitude and fluctuation taking into account of stellar emission and emission from ionized gases surrounding stars. As for the fluctuation, they predicted monotonic decrease of fluctuating power toward large angle, which is not consistent with ours. The power spectrum they posed is not caused by the distribution of dark matter but by fluctuation of halos themselves. This means mass of halo must be much less than  $2 \times 10^9$  solar mass. However, their result provides valuable information on the physical condition of early populations which is independent from halo mass.

Spectrum of the sky brightness at  $2 \sim 4 \mu\text{m}$  obtained by Fernandez et al. (2010) shows a blue color, and main emission component is attributed to stars. Furthermore, the ratio of fluctuating power to absolute sky brightness,  $\delta I/I$ , does not depend on the wavelength. This justifies to regard the spectral shape of absolute brightness to be same as that of fluctuating power. The AKARI observation shows a little bluer color than that by Fernandez et al. (2010), but is marginally consistent if we take large errors in AKARI data into account. A good correlation between wavelength bands can be explained with the simulation result that the nearest early population stars provide largest contribution to the sky brightness.  $\delta I/I$  estimated by Fernandez et al. (2010) is  $\sim 0.02$  at a few hundred arcseconds in case of the largest fluctuation. Observed fluctuation power at  $2.4 \mu\text{m}$ ,  $\sim 0.2 \text{ nWm}^{-2}\text{sr}^{-1}$ , renders absolute sky brightness to be brighter than  $\sim 10 \text{ nWm}^{-2}\text{sr}^{-1}$ , which is consistent with

excess brightness observed by IRTS and COBE (see Fig.13 in Matsumoto et al. (2005)). Fernandez et al. (2010) predicted a clear peak of the redshifted Ly $\alpha$  from the ionized gas. The wavelength of this peak depends on the redshift of nearest early population stars. Since there is no signature of redshifted Ly $\alpha$  in AKARI data, it must appear below  $2\ \mu\text{m}$ , that is, the redshift of the nearest early population stars is less than 15. Detection of the redshifted Ly $\alpha$  both in amplitude and fluctuation will be a key issue to delineate the epoch of star formation of early populations.

## ACKNOWLEDGMENTS

We thank IRC/AKARI team for their encouragement and helpful discussions. Thanks are also to Professor A. Cooray and Professor E. Komatsu for the valuable discussions. This work was supported by JSPS Grant-in-aid (18204018). HML was supported by NRF grant No. 2006-341-C00018.

## REFERENCES

- Abraham, P., Leinert, C., Acosta-Pulido, J. A., Schmidtbreick, L., & Lemke, D. 1999, in  
The Universe as Seen by ISO, Eds. P. Cox & M. F. Kessler, ESA-SP 427, p. 261
- Aharonian, F., et al. 2006, *Nature*, 440, 1018
- Arendt, R.G., & Dwek, E. 2003, *ApJ*, 585, 305
- Cambr  sy, L., Reach, W. T., Beichman, C. A., & Jarrett, T. H. 2001, *ApJ*, 555, 563
- Chary, R., Cooray, A., & Sullivan, I. 2008, *ApJ*, 681, 53
- Cooray, A., et al. 2004, *ApJ*, 606, 611
- Cooray, A., et al. 2007, *ApJ*, 659, L91
- Dwek, E., Arendt, R. G., & Krennrich, F. 2005, *ApJ*, 635, 784
- Fernandez, E., Komatsu, E., Iliev, I. T., & Shapiro, P. R. 2010, *ApJ*, 710, 1089
- Hauser, M. G., et al. 1998, *ApJ*, 508, 25
- Imai, K., et al. 2007, *AJ*, 133, 2418
- Kashlinsky, A., Arendt, R. G., Mather, J., & Moseley, S. H. 2005, *Nature*, 438, 45
- Kashlinsky, A., Arendt, R. G., Mather, J., & Moseley, S. H. 2007, *ApJ*, 654, L5
- Kelsall, T., et al. 1998, *ApJ*, 508, 44
- Levenson, L. R., Wright, E. L., & Johnson, B. D. 2007, *ApJ*, 666, 34
- Lorente, R., et al. 2008, AKARI IRC Data User Manual (version 1.4),  
<http://www.ir.isas.jaxa.jp/ASTRO-F/Observation/DataReduction/IRC/>

- Madau, P., & Silk, J. 2005, MNRAS, 359, L37
- Maihara, T., et al. 2001, PASJ, 53, 25
- Matsumoto, T., et al. 2005, ApJ, 626, 31
- Matsuura, S., et al. submitted to ApJ
- Murakami, H., et al. 2007, PASJ, 59, S369
- Onaka, T., et al. 2007, PASJ, 59, S401
- Pyo, J., et al. submitted to ApJ
- Salvaterra, R., & Ferrara, A. 2003, MNRAS, 339, 973
- Sullivan, I., et al. 2007, ApJ, 657, 37
- Thompson, R. I., Eisenstein, D., Fan, X., & Rieke, M. 2007, ApJ, 657, 669
- Thompson, R. I., et al. 2007, ApJ, 666, 658
- Totani, T., Yoshii, Y., Iwamuro, F., Maihara, T., & Motohara, K. 2001, ApJ, 550, L137
- Vrtilek, J. M., & Hauser, M. G. 1995, ApJ, 455, 677

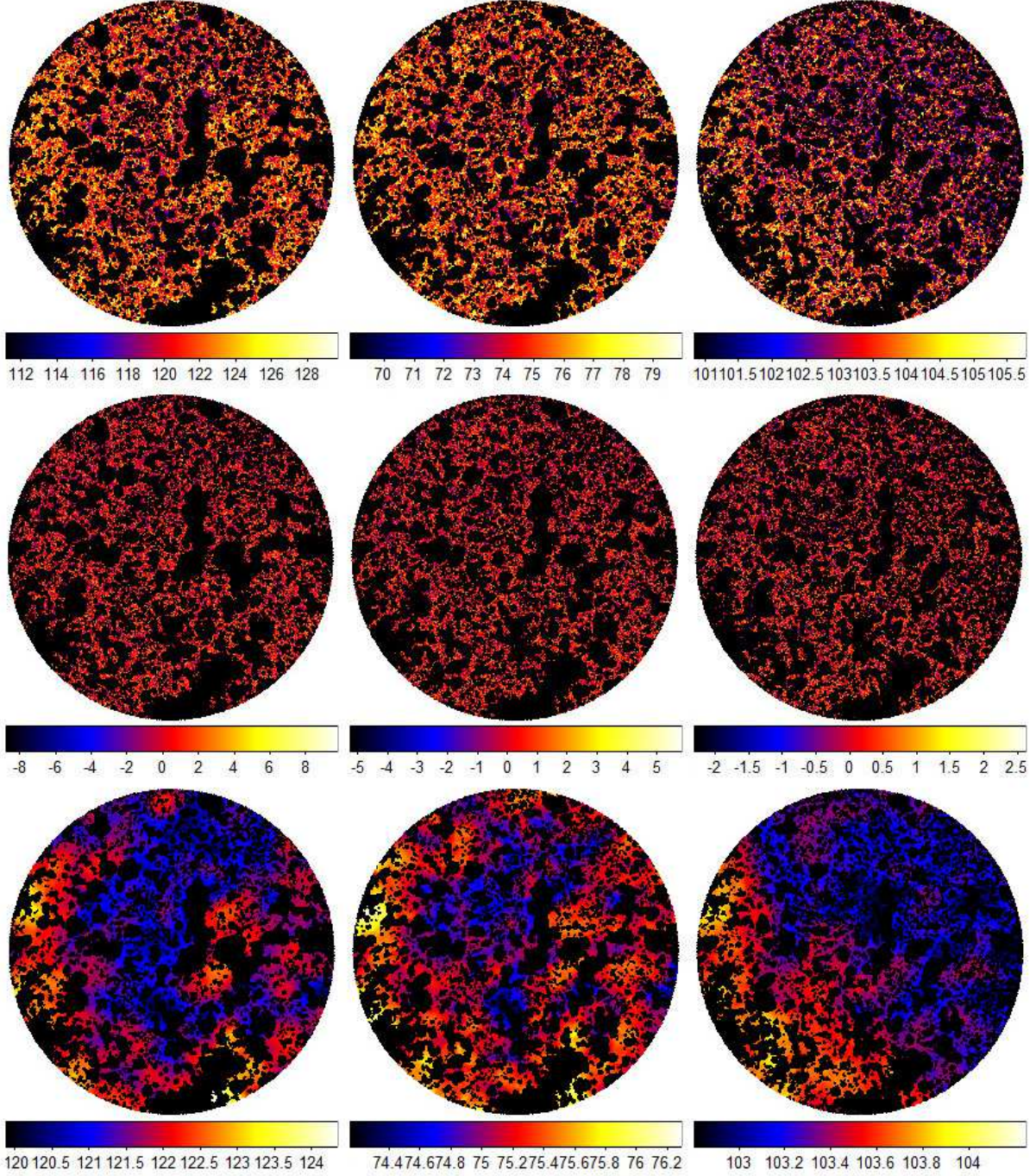


Fig. 1.— Fluctuation maps obtained by stacking. Diameter of the circles is 600 arcseconds. Maps correspond to 2.4, 3.2, and 4.1  $\mu\text{m}$  from left to right. Upper panel indicates sky maps, while middle panel shows dark maps. Lower panel shows smoothed sky maps obtained by averaging pixels within a 50 arcseconds diameter circle centered for each pixel. The unit is  $\text{nWm}^{-2}\text{sr}^{-1}$ . The color scales shown in the bar below each map are chosen so that sky maps and dark maps have a same extent of sky brightness.

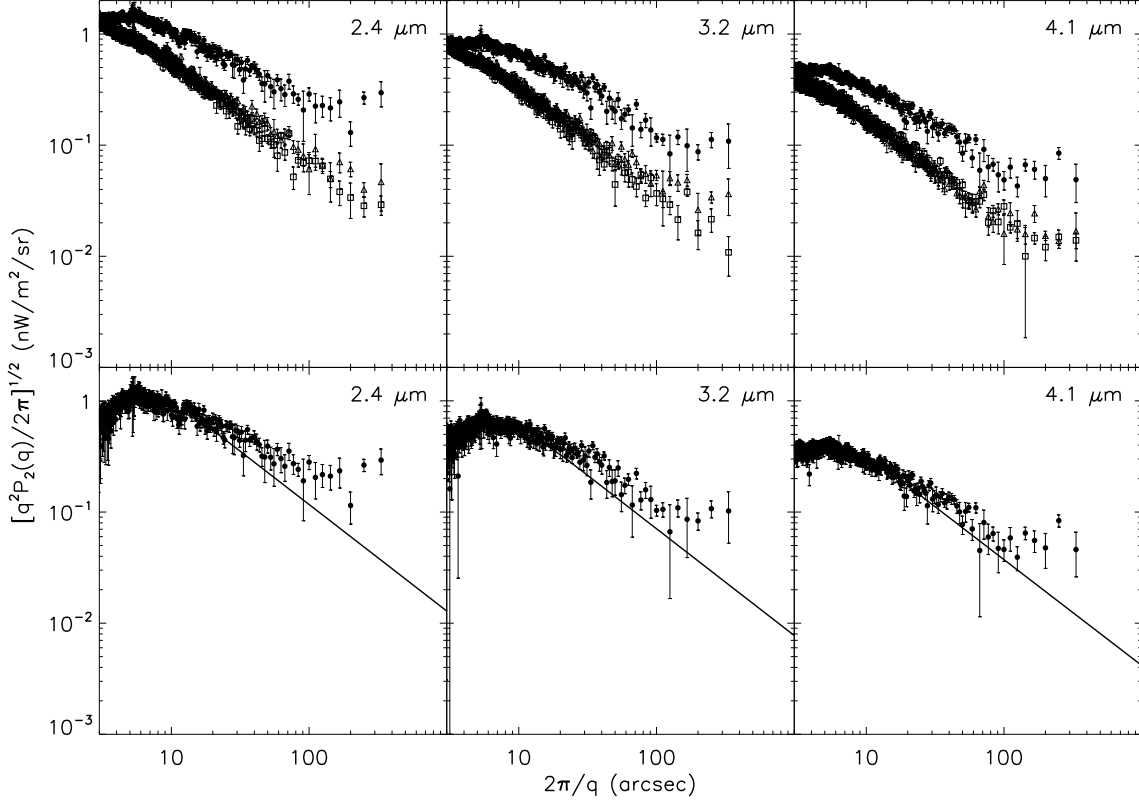


Fig. 2.— Upper panel shows power spectra,  $[q^2 P_2/(2\pi)]^{1/2}$  for sky image ( filled circles) and dark images (open triangles) in unit of  $\text{nWm}^{-2}\text{sr}^{-1}$ , obtained by two-dimensional Fourier analysis are shown as a function of angular scale  $(2\pi)/q$ . Graphs correspond to 2.4, 3.2, and 4.1  $\mu\text{m}$  from left to right. Open squares indicate the results of the subset analysis (see text). Lower panel indicates power spectra of the sky after subtracting the dark images from the sky images in quadrature. Straight lines indicate power spectra of shot noise due to unresolved faint galaxies. All error bars represent statistical errors only.



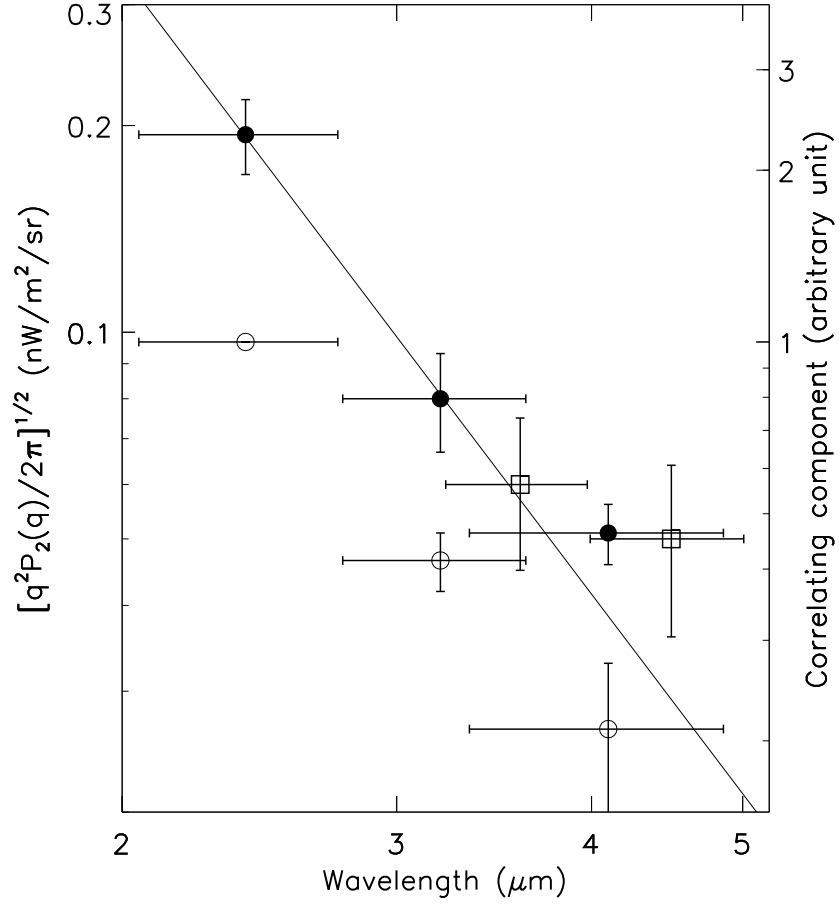


Fig. 3.— Spectrum of average power for 7 points at angular scales between 100 and 350 arcseconds is shown in filled circles. Error bars represent the statistical errors of 7 data points. Open squares show the Spitzer results. The open circles represent the spectrum of the correlating component normalized to the  $2.4 \mu\text{m}$  band. The straight line indicates Rayleigh-Jeans spectrum ( $\sim \lambda^{-3}$ ). The horizontal bars indicate bandwidth.

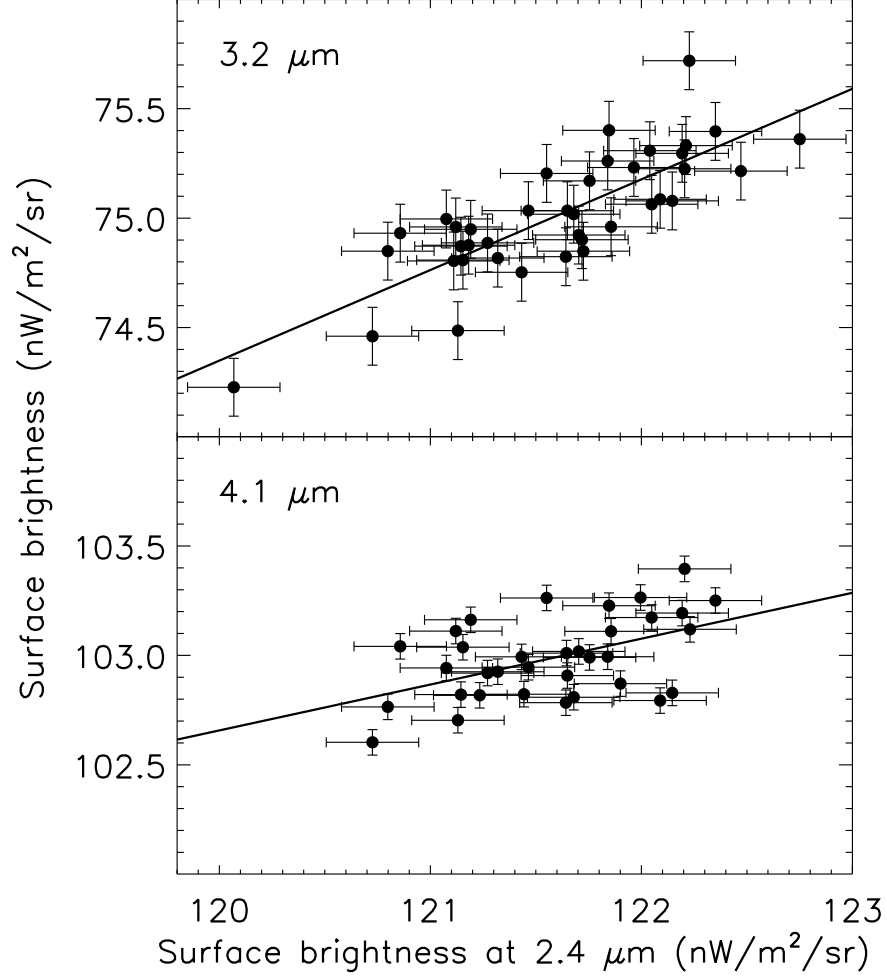


Fig. 4.— Correlation diagrams between wavelength bands for smoothed maps. Upper panel shows correlation diagram for 3.2  $\mu\text{m}$  and 2.4  $\mu\text{m}$ , while lower panel shows that for 4.1  $\mu\text{m}$  and 2.4  $\mu\text{m}$ . Only independent data points are plotted. Error bars represent standard deviations of the smoothed dark maps. The straight lines show the results of a linear fit.

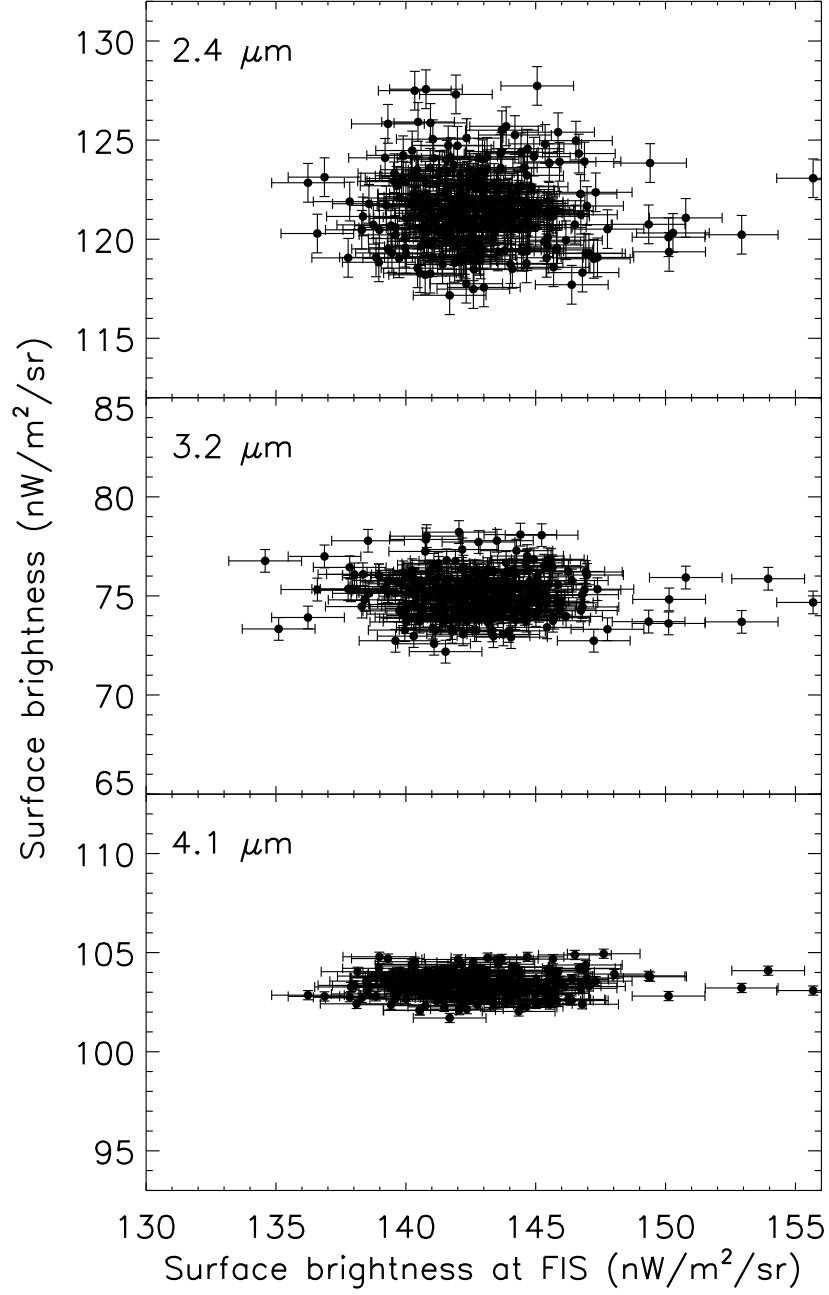


Fig. 5.— Correlation diagrams between AKARI maps and the far-infrared map (90  $\mu\text{m}$ ) observed by FIS/AKARI. The angular resolutions of the AKARI maps were degraded to that of the FIR observations, 30 arcseconds. Error bars indicate the standard deviations of the dark maps for both observations.